magnetochemistry

MDPI

Review

Perspectives on Neutron Scattering in Lanthanide-Based Single-Molecule Magnets and a Case Study of the $Tb_2(\mu\text{-}N_2)$ System

Krunoslav Prša [1], Joscha Nehrkorn [1,2], Jordan F. Corbey [3], William J. Evans [3], Selvan Demir [4,5], Jeffrey R. Long [4,6,7], Tatiana Guidi [8] and Oliver Waldmann [1,*]

1 Physikalisches Institut, Universität Freiburg, D-79104 Freiburg, Germany; krunoslav.prsa@physik.uni-freiburg.de (K.P.); nehrkorn@uw.edu (J.N.)
2 Department of Chemistry, University of Washington, Seattle, WA 98195, USA
3 Department of Chemistry, University of California, Irvine, CA 92617, USA; jcorbey@uci.edu (J.F.C.); wevans@uci.edu (W.J.E.)
4 Department of Chemistry, University of California, Berkeley, CA 94720, USA; selvan.demir@chemie.uni-goettingen.de (S.D.); jrlong@berkeley.edu (J.R.L.)
5 Institut für Anorganische Chemie, Georg-August-Universität Göttingen, Tammannstraße 4, 37077 Göttingen, Germany
6 Department of Chemical and Biomolecular Engineering, University of California, Berkeley, CA 94720, USA
7 Materials Sciences Division, Lawrence Berkeley National Laboratory, Berkeley, CA 94720, USA
8 ISIS Facility, Rutherford Appleton Laboratory, Chilton, Didcot, Oxfordshire OX11 0QX, UK; tatiana.guidi@stfc.ac.uk
* Correspondence: oliver.waldmann@physik.uni-freiburg.de; Tel.: +49-761-203-5717

Academic Editor: Kevin Bernot
Received: 8 November 2016; Accepted: 25 November 2016; Published: 14 December 2016

Abstract: Single-molecule magnets (SMMs) based on lanthanide ions display the largest known blocking temperatures and are the best candidates for molecular magnetic devices. Understanding their physical properties is a paramount task for the further development of the field. In particular, for the poly-nuclear variety of lanthanide SMMs, a proper understanding of the magnetic exchange interaction is crucial. We discuss the strengths and weaknesses of the neutron scattering technique in the study of these materials and particularly for the determination of exchange. We illustrate these points by presenting the results of a comprehensive inelastic neutron scattering study aimed at a radical-bridged diterbium(III) cluster, $Tb_2(\mu\text{-}N_2^{3-})$, which exhibits the largest blocking temperature for a poly-nuclear SMM. Results on the Y^{III} analogue $Y_2(\mu\text{-}N_2^{3-})$ and the parent compound $Tb_2(\mu\text{-}N_2^{2-})$ (showing no SMM features) are also reported. The results on the parent compound include the first direct determination of the lanthanide-lanthanide exchange interaction in a molecular cluster based on inelastic neutron scattering. In the SMM compound, the resulting physical picture remains incomplete due to the difficulties inherent to the problem.

Keywords: single-molecule magnet; lanthanide ions; inelastic neutron scattering; ligand field; Ising model; magnetic exchange

1. Introduction

Single-molecule magnets (SMMs) based on lanthanide ions offer an exciting development towards their potential practical usage, and this field has accordingly attracted enormous attention recently. In particular, large magnetic moments linked with the 4f electronic shell and large anisotropy enable higher blocking temperatures (T_B) than those previously achieved in SMMs containing transition-metal ions [1–3]. Lanthanide-containing molecules are also promising candidates in many other areas,

ranging from magneto-calorics, over exotic quantum many-body states to quantum computing [4–9]. Several excellent reviews of the field are available [10–15].

The fundamental challenges associated with lanthanide ions, concerning their theoretical description and experimental investigation, have been well established for decades [16,17]. After the seminal discovery of slow magnetic relaxation and quantum tunneling of the magnetization in the archetypical SMM Mn_{12}acetate [18,19], research on SMMs and molecular nanomagnets focused mainly on clusters containing transition metal ions. Nevertheless, the potential of incorporating lanthanide ions was soon realized. A striking example, which emerged in this period of research, is the $LnPc_2$ series of single-ion SMMs [20]. However, maybe not surprisingly, researchers largely shied away from the complexities brought in by lanthanide ions for nearly two decades. The situation changed fundamentally when it was realized that with transition-metal based SMMs the blocking temperature is not likely to be further raised substantially [21]. Further work on lanthanide-based molecular clusters followed and indeed showed novel, spectacular properties [1,3,5,6,11]. Focus shifted to the lanthanide systems, and the intense efforts have resulted in remarkable progress and achievements; this special issue is a testimony to it. However, the inherent challenges encountered in lanthanide-containing molecules, of theoretical, experimental and fundamental nature, have essentially not yet been overcome.

In the first part of this work we will discuss these challenges, addressing some aspects, which, in our opinion, deserve larger attention, without attempting to be comprehensive, as excellent complementary reviews are available [22–25]. Our emphasis is on spectroscopic techniques and neutron scattering (NS) in particular. In addition, the considerations are directed towards exchange-coupled poly-nuclear lanthanide-based compounds. We will only briefly comment on single-ion SMMs, since, in our opinion, here the advantages of NS often will not compensate for its disadvantages in comparison to other available experimental techniques.

The NS techniques have seen tremendous progress in the last decade. Throughout the world, long-term programs have been put into place to enhance NS spectrometers and explore novel NS measurement techniques. The development can thus be safely extrapolated to continue at a similar pace for the next decade. Elaborating on the current and future perspectives of NS in our research field may thus be timely, especially as only very few NS studies on lanthanide-based molecular clusters were undertaken to date [26–35].

A frequently cited difficulty with lanthanide ions is their weak exchange coupling, in comparison to what is typically found in transition metal clusters [3,12,14,15]. Indeed, according to the principles for achieving "good SMMs" with high blocking temperature derived from the studies on transition metal-based SMMs, this represents a challenge. However, in our opinion, this aspect is overstressed, since it is not a fundamental limit, and can be overcome by "better" principles. Creating single-ion SMMs is such a principle, and these indeed currently hold the world-record in terms of relaxation barrier [3]. Enhancing the apparent interaction between the lanthanide ions by incorporating non-4f magnetic electrons would be another, exploited in the family of compounds studied in this work. In addition, mixed 3d-4f clusters might deserve more attention, encouraged by the fact that nowadays essentially all hard magnets of technological relevance contain rare earth ions [36]. We will argue that the low symmetry at the lanthanide site usually found in poly-nuclear clusters poses a greater challenge, in terms of the theoretical and experimental characterization. This additional complication may not be favorable for achieving SMMs with high T_B [3,37], but might enable other peculiar magnetic phenomena [4].

In the second part of this work, as a working example, we report original results of a study designed to spectroscopically extract information on the magnetic interactions in the high-T_B $Ln_2(\mu\text{-}N_2^{3-})$ system, with Ln = Tb, Dy. The obstruction of weak magnetic coupling between magnetic moments on the 4f electrons has been overcome using a radical N_2^{3-} bridge between the lanthanide ions [1,2,38]. In contrast with their non-radical-bridged parent compounds $Ln_2(\mu\text{-}N_2^{2-})$, this procedure results in SMMs with the highest blocking temperatures observed so far in a poly-nuclear SMM

(T_B = 14 K in the $Tb_2(\mu\text{-}N_2^{3-})$ system) [1]. While the qualitative evidence for the enhanced exchange interactions is present in the low-temperature magnetization data, the quantitative description of this effect is limited to the non-SMM Gd compound (Ln = Gd) based on the isotropic $S = 7/2$ spin of the Gd^{III} ion. The INS technique can offer unique insight into this problem, because excitations based on the exchange interactions are not forbidden by selection rules and can be directly obtained. The INS experiments were conducted on three members of this series, the parent compound $Tb_2(\mu\text{-}N_2^{2-})$ (**1**), the SMM compound $Tb_2(\mu\text{-}N_2^{3-})$ (**2**), and the analogue $Y_2(\mu\text{-}N_2^{3-})$ (**3**), using the spectrometer LET at the ISIS neutron spallation source (Rutherford Appleton Laboratories, Didcot, UK) [39].

The study sheds light on the mentioned aspects. For one, this family of compounds presents an example of how to defeat the weak exchange situation. Secondly, the LET spectrometer represents a latest-generation NS spectrometer and is an example of the dramatic progress in NS mentioned before. Exploiting the time structure of the neutron pulses generated by the ISIS neutron spallation source allowed us, to put it simply, to measure the neutron spectrum for three considerably different incident energy and resolution configurations simultaneously in one run. With traditional spectrometers, one would have to undertake three measurement runs, taking approximately three times longer. This approach obviously has great potential, and the present study represents one of the first efforts to exploit it for a molecular magnetic compound [40,41]. Within this comprehensive work, we have been able to extract a meaningful physical picture for the magnetic ground state of the parent compound $Tb_2(\mu\text{-}N_2^{2-})$. A satisfactory description of the SMM compound $Tb_2(\mu\text{-}N_2^{3-})$ was not, however, possible because of the intrinsic lack of data in relation to the size of the possible parameter set.

2. General Challenges in Studying the Magnetism in Ln-Based SMMs

2.1. Experimental Aspects of Ln-Based Clusters

To set the stage, let us first comment on mono-nuclear Ln-based clusters and single-ion SMMs in particular. In these systems, the trend is clearly towards molecules with high local symmetry on the lanthanide site, since this has been identified to be crucial for enhancing the SMM property [3,37]. Only in that way "pure" ligand field levels are obtained and for example ground state tunneling can be minimized. Accordingly, the theoretical description of the experimental results by means of phenomenological models is much simplified, as the number of free parameters is much reduced. For instance, the spectroscopic data for $(NBu_4)[HoPc_2]$ and $Na_9[Tb(W_5O_{18})_2]$ could be described with 3 Stevens parameters [30,34]. The proper experimental characterization of such compounds can be a huge challenge, as the example of the $LnPc_2$ molecules shows, but the general approach essentially falls back to an extension of what has been established decades ago.

Given the $\Delta M_J = \pm 1$ selection rule [23,42] in photon-based spectroscopy (electron paramagnetic resonance (EPR), far infrared (FIR), optical, etc.), the high symmetry typically results in few allowed transitions. This is welcome, since it simplifies the analysis, but may also result in silence, for instance in the EPR spectrum. From the perspective of the observability of transitions, low symmetry environments are preferred, since the mixing of states enables more transitions to acquire finite intensity. However, here the spectra often became very complicated, especially in high-resolution techniques such as EPR, which can yield very detailed information that is difficult to extract [25].

For mono-nuclear compounds, INS is governed by the very same selection rule, and thus does not offer any fundamental advantage over the photon-based methods. INS can be, of course, very helpful in obtaining information on ligand-field levels, as it allows one to cover the relevant energy range, and does so in zero magnetic field, which avoids complications. However, there are also significant down-sides, such as low scattering intensity, resolution, absorption and background contributions (vide infra). A further, major obstacle is that INS spectrometers, and NS techniques in general, are not available in-house.

In contrast to the mono-nuclear case, NS techniques do, however, provide additional fundamentally different information when applied to poly-nuclear clusters, which are in the focus in

this work. According to the common wisdom typically presented when comparing photon-based and neutron-based spectroscopies, and INS and EPR specifically, INS offers the distinct advantage of a direct observation of exchange splitting, thanks to the INS selection rule $\Delta S = \pm 1$, while these transitions are forbidden in EPR (since here $\Delta S = 0$, where S refers to the spin angular momentum) [22,23]. While these selection rules, of course, apply also to the case of lanthanides, the conclusion as regards the observation of exchange splitting cannot be upheld. A striking recent example is the observation of the exchange splitting in the $[Dy_2(hq)_4(NO_3)_3]$ molecule using EPR techniques [43].

The fundamental advantage of NS over photon-based techniques is its ability to detect spatial distributions and correlations through the dependence of the NS intensity on the momentum transfer, **Q**. This allows us to extract information from the data, which is not accessible to photon-based spectroscopic methods, since here **Q** is practically zero, except when x-ray frequencies are reached. The distinction between NS and (non X-ray) photon-based spectroscopy is thus better cast in terms of the momentum transfer [23], which for NS is typically in the range of Q = 0.1–5.0 Å^{-1} (for cold neutron spectrometers), and $Q \approx 0$ for the photon techniques. In view of that, our distinction between mono-nuclear and poly-nuclear systems appears natural.

The greater flexibility given by the INS selection rules implies that more transitions can be observed than in the photon-based methods. In general this is much appreciated, but it also can lead to ambiguities. Although not on a lanthanide-based SMM, the work on $NEt_4[Mn^{III}_2(5\text{-}Brsalen)_2(MeOH)_2Os^{III}(CN)_6]$ provides a text-book example [44]: The INS spectra and magnetization data could be convincingly interpreted within an Ising-exchange model, but was found to be inconsistent with THz-EPR spectra, which were recorded subsequently. Only through the combination of all three techniques, explicitly exploiting the different selection rules for INS and EPR, the three-axis anisotropic nature of the exchange interaction was identified.

Poly-nuclear clusters with low site symmetry should also, in principle, allow richer spectra to be observed than in high-symmetry single-ion molecules. Nevertheless, SMMs based on lanthanide ions can pose a challenge with regard to experimentally obtainable relevant quantities. Essentially, the amount of data that reflect the interaction between the magnetic moments is small, as compared to the number of parameters to be determined in phenomenological models.

Finally, we shall comment on the experimental challenges specific to NS. The complications due to the huge incoherent background produced by the hydrogen atoms in the samples, as well as the relatively low scattering intensity of NS (especially INS), and thus the large required sample masses, are widely recognized [22,23]. The use of lanthanides adds some further complications.

In contrast to the case of 3d metals, some of the lanthanide ions exhibit a large absorption cross section for natural abundance. A comparison for some frequently encountered elements is shown in Table 1. Generally the absorption is somewhat larger than for the transition elements, but Dy, Sm, and especially Gd stand out. NS experiments on Dy compounds are possible but difficult, while they are generally infeasible for Gd compounds. This problem can be bypassed by using low-absorption isotope enriched samples of those elements. For instance, ^{163}Dy and ^{160}Gd have been successfully employed in obtaining spectra [45,46].

Table 1. Neutron absorption cross sections [in units of barns] for some metal elements for natural abundance [47].

H	Cr	Mn	Fe	Y	La	Nd	Sm	Gd	Tb	Dy	Ho	Er	Yb
0.33	13.3	2.6	3.1	1.3	9	50	5922	49,700	23	994	65	159	35

The NS intensity results not only from the magnetic moments in the sample but also from the lattice of nuclei. INS data for instance thus also contain vibrational excitations of the molecule, which need to be distinguished from the magnetic spectrum. This problem seems to be more prevalent in lanthanide containing clusters than in the transition metal clusters. This point can be addressed in several ways, for instance by a Bose correction of high temperature data to estimate the lattice

contribution, by performing the same INS experiment on analogue compounds, or substituting for example hydrogen to shift the vibrational frequencies [23,29,32,48].

All the mentioned challenges apply to the $Ln_2(\mu\text{-}N_2^{n-})$ compounds investigated in this work. In addition, these compounds are highly air sensitive, which makes them more difficult to handle experimentally, and required special precautions in the planning and undertaking of the experiments.

2.2. Challenges of Analysis

A further difficult intrinsic problem relates to the modelling of poly-nuclear lanthanide-based SMMs. Generally, the modelling is based on effective Hamiltonians containing parameters that need to be determined from experiment, or ab initio calculations (or combinations of both, as for example in the two-step CASSCF approach) [11,49].

A typical effective Hamiltonian for describing the ligand-field levels of a single lanthanide ion is composed of the Stevens operators. The low symmetry of the lanthanide site in principle requires 27 Stevens operators for describing the local anisotropy of the magnetic moment, with the same number of fit parameters (not counting the minor reduction resulting from proper standardization [25]). Notably, already in this step substantial (yet reasonable) assumptions have been made; for describing for example the $J = 15/2$ multiplet for a Dy^{3+} ion, the number of required parameters is actually 119. In addition to the ligand field parameters, terms also need to be added to the effective Hamiltonian to describe the exchange interactions. In a first attempt, when the single-ion J multiplets are considered, these often can be approximated by isotropic Heisenberg exchange [50,51], but for high accuracy also anisotropic/antisymmetric exchange components are required. Therefore, for lanthanide-containing clusters the experiments typically yield less information, while the number of phenomenological parameters is enormously increased, as compared for example to the situation in 3d-only clusters. One obvious way out of this is to consider lower-level effective Hamiltonians, which aim at describing a smaller set of states. This can be successful for describing low-temperature properties, but inevitably fails for understanding the magnetic susceptibility, or the relaxation properties of SMMs [11,37,52]. Alternatively, semi-empirical models such as the point-charge model or improved versions of it [17,24,53] can be used, which promise fewer parameters, but introduce hard to control approximations. They thus typically need to be "calibrated" by a large data set, which may not be available [24].

Ab initio calculations have improved dramatically in recent years and have proven indispensable for arriving at a deep understanding of the electronic structure in the lanthanide-based molecules [11,49]. The calculated results are impressive, yet, usually they do not match the experiments perfectly, leaving room for improvement [30,35]. However, due to the parameter-free nature of these calculations, it is far from clear which tuning knobs would need to be adjusted in order to improve the agreement with experiment. For instance, the ab initio result for the ligand field levels of a specific ion in the cluster in principle can be (and in fact have been) expressed in terms of the Stevens formalism, yielding precise values for all 27 Stevens parameters [32,49]. However, the question arises, which of them should be adjusted and how in order to better match the experimental data.

The situation is this: The effective Hamiltonian approach, which so successfully allows us to bridge the gap between experiment and (ab inito) theory, reaches its limits, as is illustrated in Figure 1. The primary culprit for the issues is the low symmetry at the metal sites, in combination with a lack of a (theoretical) understanding of the relative importance of ligand-field parameters. The latter point prevents experimentalists from choosing minimal yet sensible combinations of parameters in their effective Hamiltonians, and work aimed at overcoming this would, in our opinion, open a path for improving the situation.

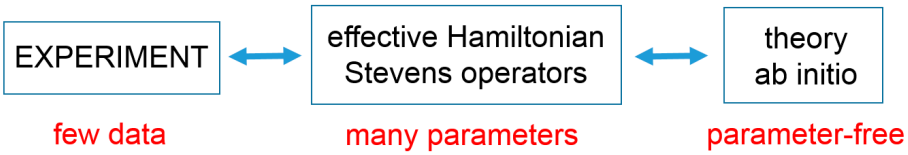

Figure 1. Sketch of the interconnection of challenges in the experimental studies of lanthanide-based systems (for details see text).

2.3. Perspectives of Neutron Scattering Techniques

The lanthanide (Ln^{III}) ion chemistry enables careful studies of entire families of compounds with the same ligand environments. The ligand fields are little affected by chemical substitution and ligand field parameters, when corrected with for example the Stevens parameters, should be largely transferable within a family. This long-known approach has been exploited for instance in inferring the ligand field in the $LnPc_2$ family from NMR and magnetization data [20]. It should be also suitable for systematic NS studies.

We suggest that NS studies on single crystals of molecular magnets should become more commonplace in the future. When using single crystals, INS allows mapping of the full scattering cross section $S(Q,\omega)$, bringing a new light to spin-spin correlations in these materials [54–56]. Similar arguments apply to other NS techniques. In fact, the modern research in quantum magnetism would not be possible if it would not be accompanied by strong efforts in crystal growing. While the necessary tools from the experimental side are present, the main challenge is on the chemists' side: hence, we call for effort to be invested in production of larger single crystals. Such efforts have indeed become accepted as a scientific necessity in the field of quantum magnetism, and we hope they will also become more accepted in our field of research.

The scattering of polarized neutrons is sensitive to both the magnetic nature of the sample, as well as to the directions of its magnetic moments. This experimental fact has been used for a long time to map magnetization densities, for example in magnetic clusters [57,58], and to solve difficult magnetic structures in extended, magnetically ordered systems. Recently, polarized neutron diffraction was applied to probe local anisotropy axes in single-crystal samples of the highly anisotropic transition metal clusters [59,60], leading to a better understanding of the interplay between the ligands and the magnetic properties. This technique is also applicable to lanthanide containing clusters, as well as even more involved polarized NS techniques, such as polarized inelastic neutron scattering.

More parameters are also available in the sample environment. While exchange can be determined using INS without the application of the magnetic field, unlike in many other techniques (e.g., EPR), magnetic fields of up to 17 T are standardly available on neutron sources. Neutron scattering samples can also be placed into pressure cells, and submitted to uniaxial or hydrostatic pressures [23].

All the mentioned techniques and approaches are going to benefit significantly from the availability of new generations of sample environments, such as for example the recently constructed 26 T magnet in the Helmholtz Zentrum Berlin, more advanced instruments, for example LET, as well as the suite of instruments planned to be constructed at the high-flux European Spallation Source (ESS). This will allow for smaller samples, more extreme conditions, systematic studies of larger sample families, and will lead to higher throughput of experimental results. The new developments are going to benefit the neutron scattering community as well as the molecular magnetism field as a whole.

3. Inelastic Neutron Scattering Study of the $Tb_2(\mu\text{-}N_2)$ System

3.1. Introduction to the $Tb_2(\mu\text{-}N_2)$ System

The compound $[K(18\text{-crown-}6)(THF)_2][\{[(Me_3Si)_2N]_2(THF)Tb\}_2(\mu\text{-}\eta^2\text{:}\eta^2\text{-}N_2)]$ (**2**), or $Tb_2(\mu\text{-}N_2^{3-})$ in shorthand, shows SMM behavior with a blocking temperature of ~14 K [1]. It is derived from a parent compound $\{[(Me_3Si)_2N]_2(THF)Tb\}_2(\mu\text{-}\eta^2\text{:}\eta^2\text{-}N_2)$ (**1**) [61], or $Tb_2(\mu\text{-}N_2^{2-})$ but differs by having

one fewer electron on the dinitrogen bridge. In addition, $[K(18crown\text{-}6)(THF)_2]^+$ cations are present in the crystal lattice of **2**, which will be of importance in what follows. The family of compounds also includes the Dy^{III}-containing molecules $Dy_2(\mu\text{-}N_2^{2-})$ and $Dy_2(\mu\text{-}N_2^{3-})$, the Gd^{III}-containing molecules $Gd_2(\mu\text{-}N_2^{2-})$ (**4**) and $Gd_2(\mu\text{-}N_2^{3-})$ (**5**), and the Y^{III} analogue $Y_2(\mu\text{-}N_2^{3-})$ (**3**) [2].

Figure 2 shows the molecular structures of the parent and derived SMM molecules **1** and **2**. The cores of **1** and **2** consists of two Tb^{III} ions ($J = 6$, $g_J = 1.5$) coupled via dinitrogen bridges N_2^{2-} and N_2^{3-}, respectively. In both compounds, the Tb sites are occupying a crystallographically equivalent but low-symmetry site. The additional electron on the dinitrogen bridging unit in the SMM compound **2** is considered to increase the magnetic coupling strength significantly [1,2]. Indeed, fits to the magnetic susceptibility of the Gd^{III} compounds **4** and **5** yielded coupling strengths of $\mathcal{J} = -1.4$ K and $\mathcal{J} = -78$ K (in $\mathcal{J}$ notation), respectively, as well as evidence for a weak intermolecular interaction of $\mathcal{J}'$ in **5** [1]. These compounds are not suitable for INS studies due to the large neutron absorption cross sections for natural Gd, as discussed above.

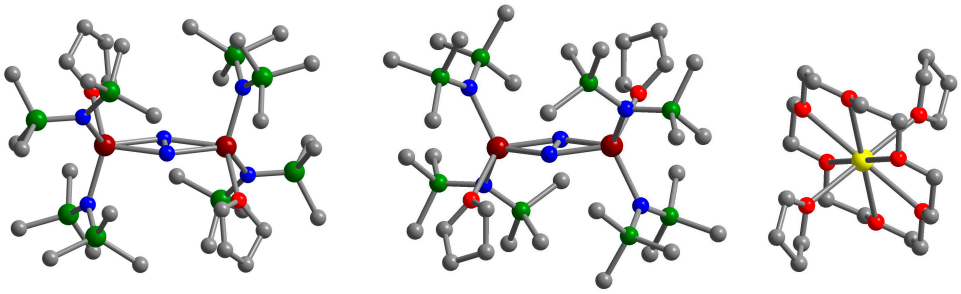

(**a**) (**b**)

Figure 2. (**a**) Molecular structure of the parent compound $Tb_2(\mu\text{-}N_2^{2-})$ (**1**); (**b**) Molecular structure of the SMM (single-molecule magnet) compound $Tb_2(\mu\text{-}N_2^{3-})$ (**2**). In both panels: Tb^{III} in dark red, N in blue, O in light red, Si in green, C in gray, K in yellow, H atoms were omitted.

The molar magnetic susceptibilities of the parent and SMM compounds **1** and **2** were reported previously [1]. The magnetic susceptibility of the parent compound **1** is shown in Figure 3a. The χT vs. T curve grows monotonically from a low value of 3.4 cm^3K/mol at the lowest temperature of 2 K and flattens out at high temperatures approaching the Curie value of 23.62 cm^3K/mol. An overall down turn of the χT curve with lowering temperature is typical for ligand-field levels of lanthanide ions, but for Tb^{III}, the curve should approach a significant finite value at zero temperature in a pure ligand field model [16,17]. The drop to nearly zero at the lowest temperatures is consistent with a weak antiferromagnetic exchange interaction between the Tb^{III} magnetic moments.

The molar magnetic susceptibility χT vs. T of the SMM compound **2**, for temperatures above its blocking temperature, is shown in Figure 3b. At 300 K the χT value is 22.9 cm^3K/mol. As the temperature is lowered, the susceptibility grows, which is expected for the effective ferromagnetic alignment between the Tb^{III} magnetic moments. The data show a broad maximum at about 70 K, reaching a χT value of 34.6 cm^3K/mol, followed by a decrease at lower temperatures, with $\chi T = 31.0$ cm^3K/mol at 15.6 K. The down turn could suggest the presence of excited states in the energy range of ca. 70 K with higher magnetic moment than the ground state, which get depopulated at low temperatures. An alternative could be the presence of weak antiferromagnetic intermolecular interactions (vide infra).

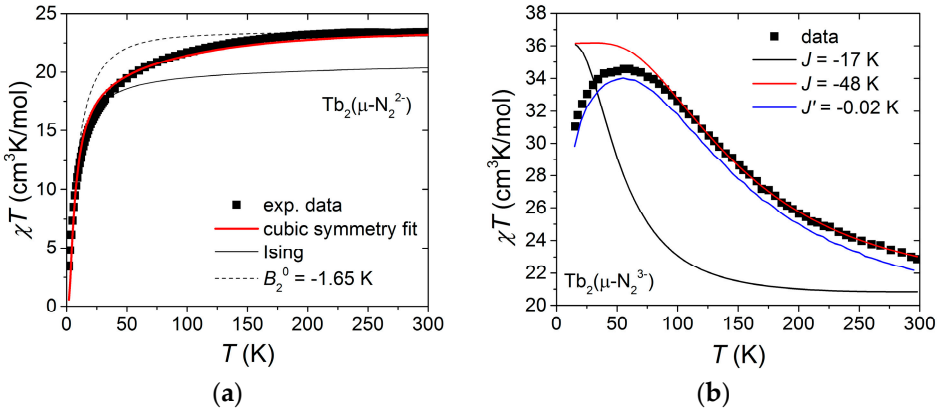

Figure 3. (**a**) Molar magnetic susceptibility data (squares) of the parent compound **1** collected at 1 T and the calculations (lines) based on the three models discussed in the text; (**b**) Molar magnetic susceptibility of the SMM compound **2** (squares) and the calculations (lines) based on several models discussed in the text.

3.2. Experimental Details

In order to determine the thermodynamic magnetic behavior in the ground state of the parent compound **1**, field-dependent magnetization curves were recorded. The maximum field was 7 T, and temperature ranged from 2 K to 20 K.

In view of the expected challenges with studying and analyzing the magnetism in the SMM compound **2**, as described previously, it is fortunate that the parent compound **1** and the analogue with diamagnetic Y^{III}, **3** are also available, as each can yield important insights into the vibrational background and the exchange couplings in the SMM complex in **2**. The INS experiments, using the LET spectrometer at the ISIS facility, were therefore conducted on all three compounds. Regarding the comparison of results, it should be noted, however, that the vibrational spectrum for the parent compound **1** can be expected to be very different from those for the compounds **2** and **3**, due to the presence of the K-crown cations in the latter. In addition, the additional charge on the dinitrogen bridge in **2** should significantly affect the ligand field at the Tb^{III} sites in this compound. The ligand fields in **1** and **2** are thus not comparable, which must not be overlooked.

The INS spectra were measured in three energy ranges with incident neutron energy of 2 meV (low-energy range), 11 meV (intermediate-energy range), and 22 meV (high-energy range). Positive energies refer to neutron energy loss. The temperatures were varied from the base temperature of 2 K to 100 K, in several steps. The data permitted analyzing the full $S(Q,\omega)$ plot. The integrated INS intensity as a function of energy is shown for selected measurement conditions; some additional results are presented in the SI.

3.3. Magnetization Data for the Parent Compound **1**

The low-temperature magnetization data for the parent compound **1** are shown in Figure 4. At 2 K, the magnetization displays an inflection point at about 1 T and then grows rapidly until about 5 T, but does not fully saturate even at the maximum field of 7 T. The higher temperature data gradually wash out the low-field inflection feature and display an even bigger obstacle to saturation. The low-field inflection point is an indication of weak antiferromagnetic exchange interactions between the two Tb^{III} ions in the cluster. For an isolated $\pm M_J$ doublet, the powder-averaged saturation magnetization is calculated to be approximately $1/2\mu_B g_J M_J$ or ~9 μ_B for Tb^{III} and $M_J = J = 6$. The observed maximum magnetization at 7 T of 9.21 μ_B thus strongly suggests a $M_J = \pm 6$ doublet for the Tb^{III} ground state. This finding is consistent with the expectation from electrostatic considerations [10].

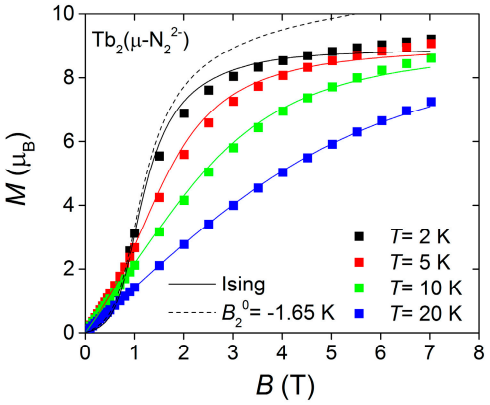

Figure 4. Magnetization data (squares) at different temperatures for the parent compound **1** and the calculations (lines) based on two models discussed in the text. The colored solid lines represent the results for the Ising model at temperatures of 2, 5, 10, 20 K (black to blue). The dashed line represents the result for Equation (2) at 2 K.

3.4. Inelastic Neutron Scattering Data for the Parent Compound **1**

Figure 5a shows the temperature dependence of the low-energy INS spectrum collected for the parent compound **1**. The main feature is a clear excitation at 0.75 meV (peak I). Its intensity decreases at higher temperatures on the neutron energy-loss side, and shows the corresponding temperature dependence on the neutron energy-gain side, which is typical for a cold magnetic transition. In addition, this peak is present at low momentum transfer Q, which rules out a phononic origin (see Figure S1). Thus, peak I, and its anti-Stokes companion peak I′, can be unambiguously assigned to a cold magnetic transition at 0.75 meV.

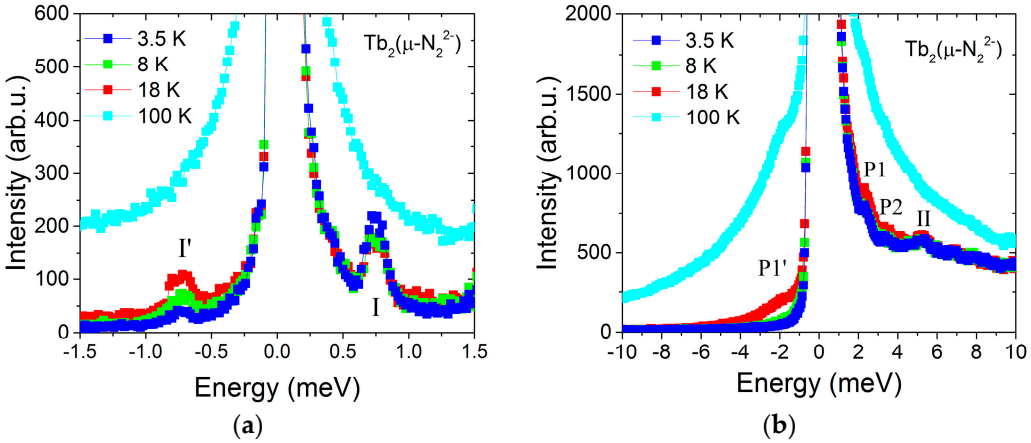

Figure 5. (**a**) Low-energy INS spectrum in the parent compound **1**. Peak I indicates the exchange-based transition and I′ its anti-Stokes pair; (**b**) Intermediate-energy levels in the parent compound **1**. Peaks P1 and P2 denote vibrational levels with P1′ the anti-Stokes pair of P1. Peak II indicates a ligand-field transition at 5.2 meV.

The intermediate-energy data shown in Figure 5b display additional levels at about 2 meV (peak P1), 3 meV (peak P2) and 5 meV (peak II). Based on the temperature dependence, only peak II behaves as a magnetic transition, which could be cold or emerge from a possibly very-low lying excitation. The intensity of this transition is large even at low Q, which is further strong evidence for a magnetic origin of the peak (see Figure S2). Based on the temperature and Q dependence, the 2 meV and 3 meV transitions are assigned to lattice vibrations (since, for example, the 2 meV transition grows on both sides with temperature).

No additional magnetic peaks could be identified in the high-energy data. From the INS data, the presence of two cold magnetic transitions in **1** is thus concluded, at 0.75(2) meV (peak I) and 5.2(2) meV (peak II).

3.5. Inelastic Neutron Scattering Data for the SMM Compound **2** *and* Y^{III} *Analogue* **3**

Figure 6a shows the intermediate-energy range INS data at base temperature for the SMM compound **2**, together with the data for its analogue containing diamagnetic Y^{III} centers, **3**. There are several peaks in this energy range. However, comparing the data of **2** with that of compound **3** enables the exclusion of most of the observed spectrum as vibrational. In **2**, there is one clear excitation at ~9 meV (peak I), which is not present in compound **3**, and can hence be assigned to a magnetic origin. There is an additional candidate for a magnetic transition at ~8.5 meV (indicated by the question mark), but if it exists it coincides with large vibrational background peaks. With the present data it cannot be identified unambiguously.

Figure 6b presents the measured temperature dependence for compound **2**. The intensity of peak I decreases at higher temperatures, which is a clear signature of a cold magnetic transition. This peak could not be seen well in the $S(Q,\omega)$ plot due to its low intensity, and thus no conclusions concerning its origin could be drawn from its Q dependence. Additionally, Bose corrections did not yield good estimates of the backgrounds (see Figure S3).

Further magnetic scattering intensity could not be identified in either the low-energy or the high-energy data. The INS experiments performed on **2** thus provide evidence for one cold magnetic transition at 9.2(2) meV (peak I). The existence of this transition plays a discerning role in the analysis below. However, the experimental evidence is, admittedly, not extremely strong. For that reason the available INS data were analyzed repeatedly with the greatest care, and it was concluded that it is of magnetic origin, but a word of caution is appropriate.

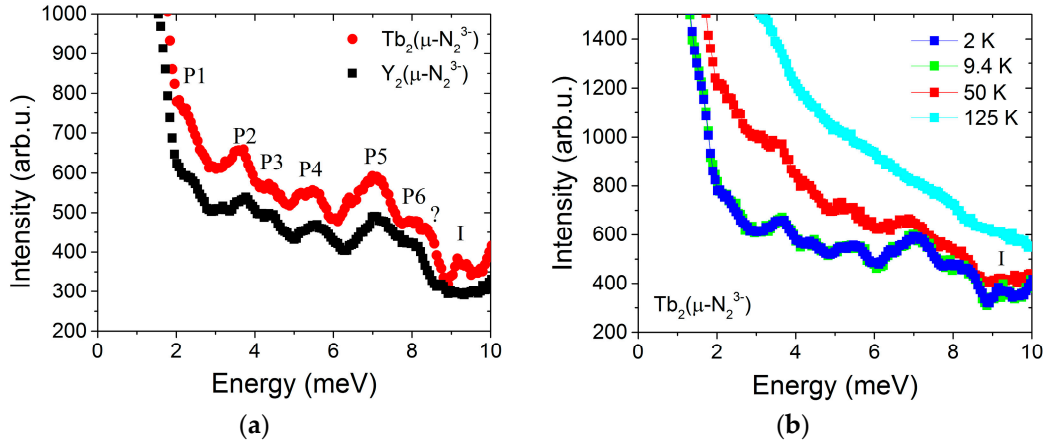

Figure 6. (**a**) Intermediate-energy INS data at 2 K in the SMM compound **2** (red) compared to the vibration spectrum in the analogue containing diamagnetic Y^{III}, **3** (black). The peaks labelled P1–P6 denote vibrational excitations seen in both compounds. The peak I at 9.2 meV is indicated; (**b**) Intermediate-energy INS spectra measured for **2** at different temperatures. Note the offset on the *y* axis in these plots, demonstrating a large incoherent scattering background.

4. Discussion

4.1. Insights from the Point Charge Model

In order to gain understanding of the single-ion properties of the investigated systems, a set of point-charge model calculations [17,53] were performed. Importantly, this simple model was not used as a quantitative device for accessing exact parameters of the local Hamiltonian. In contrast, we sought

to obtain generic information about the spectra and the single-ion wave functions for qualitative results as the low symmetry of the Tb^{III} site makes the problem intractable. For this purpose, the Tb^{III} environment was first approximated by a tetrahedral charge environment as shown in Figure 7, with two of the charges variable (representing the N_2^{n-} bridge, with $n = 2$ or 3, and the difference between the oxygen and nitrogen ion charge).

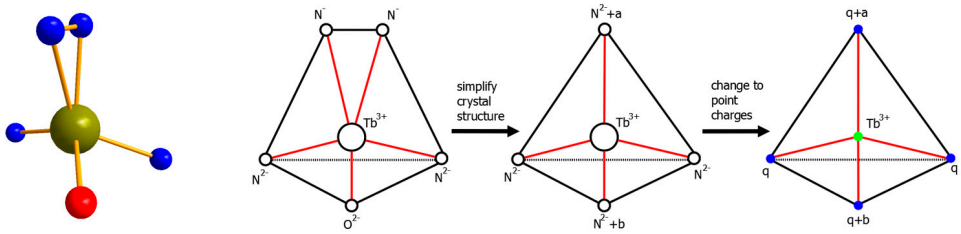

Figure 7. The local low-symmetry environment of the Tb^{III} ion and its reduction to an approximate two-parameter point-charge model, which captures the most relevant generic aspects.

The generic result of this procedure is shown in Figure 8. The Tb^{III} ion, surrounded by a polar environment, displays a non-Kramers doublet spectrum, with an approximate $M_J \approx \pm 6$ ground state, followed by an excited $M_J \approx \pm 5$ doublet ("doublet" is henceforth used to denote a non-Kramers doublet). The dominant components of the single-ion wave function pair are in the $M_J = +6$ and $M_J = -6$ sectors. However, there are small contributions to the other M_J components, which are essentially given by the symmetry of the ion's environment. For example, in a polar tetrahedral environment ($b = 0$, $a < 0$ in Figure 7), the ground state contains small $M_J = \pm 3$ and $M_J = 0$ components, as shown in Figure 8b. In the case of a low symmetry for the Tb^{III} ion, as in the studied compounds, *all* of the single-ion components have finite values, albeit much smaller than the dominant component.

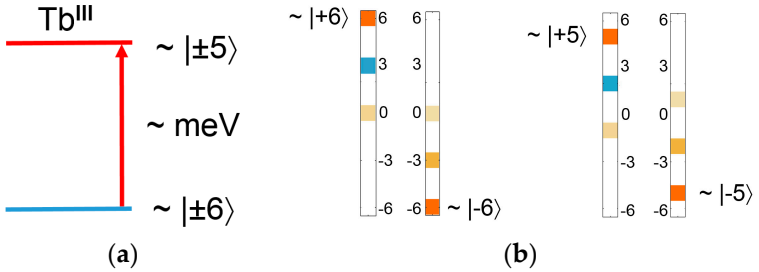

Figure 8. (**a**) The typical single-ion low energy spectrum with non-Kramers doublet single-ion wave functions of the Tb^{III} ion coming from the approximate ligand environment discussed in the text; (**b**) The bars to the right and left represent the wave functions of the $M_J \approx \pm 6$ and $M_J \approx \pm 5$ doublets in a polar tetrahedral environment, respectively, with the magnitude of the individual M_J components colour coded (red = 1, white = 0, blue = −1). In lower symmetry, the "white" components would all gain finite values.

This is an important observation for neutron scattering: The $\Delta M_J = \pm 1, 0$ INS selection rule permits INS transitions between the $M_J \approx \pm 6$ ground and $M_J \approx \pm 5$ excited ligand field states, but it would result in zero INS scattering intensity for exchange-split states if the levels were pure M_J states, as in Ising exchange models. As will be shown in detail below, if the exchange is of Ising-type, then the excitations resulting from the exchange interaction correspond to spin flips with a large associated change of the z component of the magnetic moment J^z, or M_J in fact. For instance, a transition involving a spin flip from $M_J = -6$ to $M_J = +6$ emerges, for which $\Delta M_J = 12$. However, since there are non-zero components of the initial and final states that produce $\Delta M_J = \pm 1, 0$ overlaps, it is possible to observe weak intensity in INS corresponding to these exchange-split transitions.

A further generic result of the point-charge investigation is that the lowest excitation is several meV above the ground state, and that the additional charge on the radical bridge in the SMM compound strongly shifts the ligand-field levels to even higher energies. For instance, the lowest excitation shifts from a ~6 meV range to a ~60 meV range. In other words, the magnetic system is expected to become much more anisotropic and Ising type as the competing states are pushed further away in energy. Hence, we expect that for the description of low-temperature thermodynamic quantities, we may restrict ourselves to the ground state doublet of the system, especially in the SMM compound **2**.

4.2. The Parent Compound **1**

The parent compound is described in terms of a Heisenberg spin Hamiltonian:

$$H = -\mathcal{J}\ J_1 \cdot J_2 + \sum_{i=1,2} \sum_{k=2,4,6} \sum_{q=-k}^{k} B_k^q O_k^q(i) \tag{1}$$

Here, the first part describes the usual exchange interaction between the two Tb^{III} ions, and the second part describes all the possible contributions to the ligand field in terms of the Stevens operator formalism [16,17,53]. The exchange interaction between the J multiplets of lanthanide ions can generally be well described by isotropic Heisenberg exchange [50]. Due to the large magnetic moments and weak exchange in lanthanide ions, dipolar interactions can also be appreciable [16]. These are neglected here also, because their effects are similar to those of the ligand field terms and difficult to discern. Due to the aforementioned fundamental problems with the quantity of data and the results of the point charge modelling, a much reduced Hamiltonian was also considered:

$$H' = -\mathcal{J}\ J_1 \cdot J_2 + \sum_{i=1,2} B_2^0 O_2^0(i) \tag{2}$$

The uniaxial anisotropy operator $O_2^0(i)$ allows us to mimic the effect of the ligand-field environment on the low-temperature properties of the system. The advantage of this reduction is, of course, that the Hamiltonian H' contains only two parameters.

In case of a strong Ising-type anisotropy or large negative value of B_2^0, the Hamiltonian of the system essentially reduces to a low-temperature dimer model with pure Ising exchange interactions. In Section 3.4 above, the low-temperature susceptibility and magnetization was found to indicate small antiferromagnetic interactions present in the system. The ground state and lowest exchange-split excitations in such an Ising dimer stem from the single-ion $M_J \approx \pm 6$ doublets, as indicated in Figure 9b. The lowest excitation from the ground state corresponds to a spin flip on one site and has an excitation energy of $\Delta E = 72|\mathcal{J}|$. Let us compare the results of this model to the experimentally observed excitations shown in Figure 9a: Association of the observed 0.75 meV magnetic peak with this transition results in $\mathcal{J} = -0.12$ K. Note that also in the Gd^{III} compound **4**, antiferromagnetic intra-molecular interactions were inferred [2], of strength $\mathcal{J} = -1.41$ K, which is qualitatively consistent with our finding for **1**.

In Figures 3a and 4, simulations of the magnetization and susceptibility curves are shown using the determined value of the interaction and Equation (2) with variation of B_2^0. For infinitely large B_2^0, the model reduces to that of a dimer of two-level states with pure Ising interactions and contains only one parameter, namely $\mathcal{J}$. With $\mathcal{J}$ taken from our INS results, this establishes a parameter-free model for the low-temperature magnetism in **1**. The resulting simulations are shown as solid lines in Figures 3a and 4. Remarkably, the measured magnetization is very well reproduced, demonstrating the validity of this model for the ground-state properties of **1**. The susceptibility is well reproduced at low temperatures, but strongly deviates above ~30 K (see Figure 3a). This is expected, since the ligand-field levels that govern the magnetism at higher temperatures are not present in the model (they are shifted to infinite energy by the infinite B_2^0).

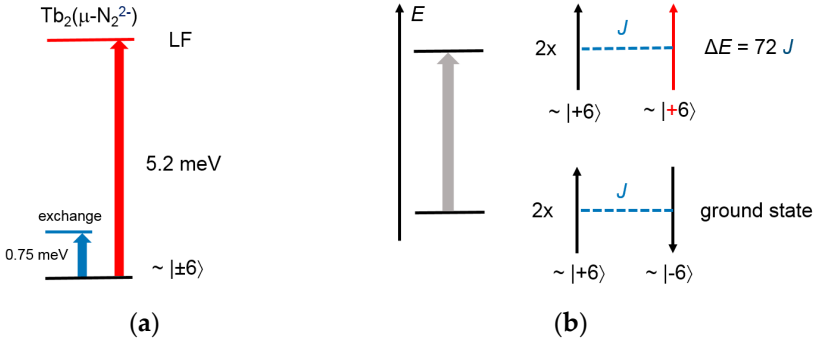

Figure 9. (**a**) Excitation energy scheme experimentally observed in the parent compound **1**; (**b**) Theoretically expected excitation spectrum of an Ising dimer formed by two exchange-coupled $M_J \approx \pm 6$ doublets. A weak INS transition occurs due to the small M_J components in the involved states, as discussed in the text.

In the next step, the value of $B_2^0$was thus chosen such that Equation (2) reproduces the observed excitation at 5.2 meV, yielding $B_2^0 = -1.65$ K. The simulated susceptibility curve (dashed line in Figure 3a) now correctly approaches the Curie value at high temperatures, but otherwise reproduces the data poorly, showing χT values that are too large in the intermediate temperature range of ~70 K. In addition, the description of the high-field part of the magnetization is worse (dashed line in Figure 4). Obviously, the magnetic contribution of the first excited ligand-field level at 5.2 meV is significantly overestimated in this model.

It is possible to obtain a relatively good fit to the magnetic susceptibility data using an extended set of Stevens operators in addition to the exchange. The red curve in Figure 3a was calculated assuming an approximate local cubic environment, with $B_2^0 = -640(27) \times 10^{-2}$ K, $B_4^0 = -77(11) \times 10^{-4}$ K, and $B_4^3 = -84(32) \times 10^{-4}$ K. However, this by no means was the only reasonable fit we found. In fact, similar fits were obtained with substantially different sets of Stevens parameters, which underpins the well-known challenges with over-parametrization in the fitting of experimental susceptibility curves. The lowest ligand field levels expected from these fits occur at around 25 meV, much larger than observed 5.2 meV peak, pointing again to the low magnetic moment associated with this excitation.

4.3. The SMM Compound **2**

The main difference, from the view point of magnetic modeling, between the parent compound **1** and the SMM compound **2** is that the magnetic exchange acts via a $s = 1/2$ electron spin on the radical dinitrogen bridge, which changes the form of the Hamiltonian to:

$$H_{SMM} = -\mathcal{J}\ (J_1 \cdot s + s \cdot J_2) + \sum_{i=1,2} \sum_{k=2,4,6} \sum_{q=-k}^{k} B_k^q O_k^q(i) \quad (3)$$

An exchange directly between the Tb^{III} ions is not included, since it can be safely assumed to be much smaller than the exchange to the radical spin and showed negligible effects in test simulations. Again, based on similar arguments as before, a simplified model of the system is considered:

$$H'_{SMM} = -\mathcal{J}\ (J_1 \cdot s + s \cdot J_2) + \sum_{i=1,2} B_2^0 O_2^0(i) \quad (4)$$

In a situation with large Ising-type anisotropy (B_2^0 very large), one expects that, in the ground state, the Ising-like moments of the Tb^{III} ions remain parallel. If the interaction $\mathcal{J}$ is antiferromagnetic, then in the ground state the radical spin s is essentially antiparallel to the Tb^{III} moments and parallel in the ferromagnetic case. The first excitation of the system corresponds to a spin-flip of a Tb^{III} moment and occurs at an energy of $\Delta E = 6|\mathcal{J}|$. A second excitation emerges at an energy of $\Delta E = 12|\mathcal{J}|$, which is related to a spin flip of the central radical spin. The exchange-split level diagram is depicted

in Figure 10b. In our INS data, we observed a single magnetic peak at 9.2 meV. If this were associated with the lowest exchange-based excitation, an exchange constant of $\mathcal{J} = -17$ K would result.

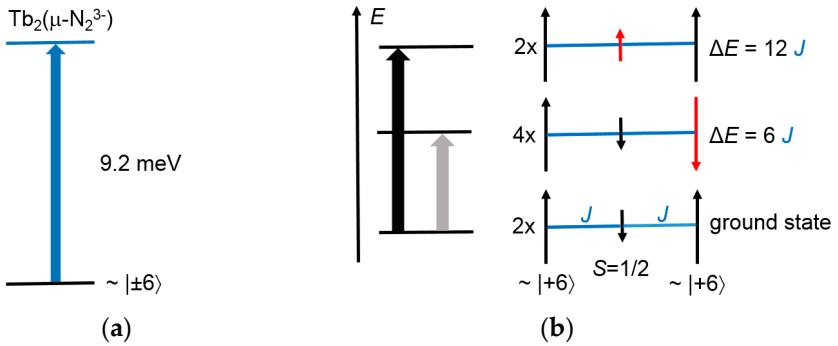

Figure 10. (**a**) Excitation energy scheme experimentally observed in the SMM compound **2**; (**b**) Theoretically expected excitation spectrum for the Ising-exchange model of the SMM compound **2** discussed in the text as a basic model. The INS transitions from the ground state to the second excited state is allowed (black arrow). A further weak INS transition from the ground state to the first excited state occurs due to the small M_J components in the involved states, as discussed in the text.

Figure 3b compares the calculation based on this value (black solid line) to the experimental susceptibility data [1]. The agreement is poor due to a significant underestimation of the exchange constant. Indeed, if one assumes an antiferromagnetic exchange interaction about three times larger of $\mathcal{J} = -48$ K (red solid line) one gets fairly good agreement with the experimental curve at higher temperatures. At present, the cause of this discrepancy is unclear. Note that associating the observed 9.2 meV transition with the expected excitation at $\Delta E = 12|\mathcal{J}|$, which could have stronger INS intensity, worsens the situation by another factor of two.

The assumed model is certainly simplified, but based on the generic findings from the point-charge considerations and the overall SMM character of the system at low temperatures, one would expect the Ising-type anisotropic model to hold better than in the parent compound **1**. An exchange-based excitation lower than $6|\mathcal{J}|$ cannot arise in such models. Interestingly, the tripled exchange coupling, $\mathcal{J} = -48$ K, is more consistent with the exchange interaction observed in the related Gd^{III} compound **5**, and moreover predicts a first excitation at 24.8 meV or 290 K, in close agreement with the energy barrier of 330 K inferred from ac susceptibility measurements performed on **2** [1]. On the other hand, this ~25 meV excitation would then indeed be the lowest excitation, and the observed INS peak at 9.2 meV would remain unaccounted for, as well as the observed significant down turn of the magnetic susceptibility at temperatures below ~70 K. The latter would indicate a ground state of the Tb^{III} ions which has a lower magnetic moment than the $M_J \approx \pm 6$ doublet emerging in any model based on a strongly Ising-type anisotropy.

These discrepancies and the decrease of the susceptibility at lower temperatures suggest the possibility of antiferromagnetic intermolecular interactions [2,62]. In a molecular field approach, this scenario yields the susceptibility $\chi = \chi_{SMM}/(1 + \lambda\chi_{SMM})$, where χ_{SMM} is the calculated susceptibility of an isolated $Tb_2(\mu\text{-}N_2^{3-})$ unit, which fits the experimental curve remarkably well with λ = 0.06 mol/emu. In an attempt to establish a more realistic model, we connect the trimeric units into a ladder configuration assuming the intermolecular couplings of $\mathcal{J}'$ only between the Tb^{III} moments. Quantum Monte Carlo simulations using the ALPS framework [63,64] were performed, with the ladder length set to 20 molecules. As shown in Figure 3b, the addition of a small intermolecular interaction of $\mathcal{J}' = -0.02$ K (blue solid line) is able to reproduce the observed low-temperature decline in the magnetic susceptibility. The origin of this effect may be the dipole-dipole interactions between the Tb^{III} moments of neighboring molecules, which are estimated to ~0.05 K, and therefore could account for the required magnitude of $\mathcal{J}'$ [2]. The intermolecular interactions give rise to an associated,

nearly dispersion-less excitation at $288|\mathcal{J}\prime| = 0.5$ meV, which is too low to account for the 9.2 meV excitation seen in INS, and no INS feature was observed at this energy.

5. Materials and Methods

Neutron scattering: Non-deuterated powder samples were synthesized following published procedures [1]. Sample shipment and handling was undertaken very carefully because of the known air sensitivity of the compounds. Cooled and sealed samples were directly shipped to the ISIS facility at the Rutherford Appleton Laboratory in Chilton, UK, and were stored in a freezer at -40 °C. Samples were wrapped into aluminum foil and mounted in the standard cans used at ISIS, all within a glovebox. Each sample was prepared shortly before the experiment, and quickly inserted into the Orange cryostat and cooled down. The sample quantities were weighed and found to be 0.834 g for **1**, 0.914 g for **2** and 1.516 g of **3**. Data were collected at the LET time-of flight neutron spectrometer at the ISIS neutron source in a multi-rep mode, in which multiple Q-energy windows can be obtained from a single measurement. Several settings were used in order to obtain an overview in Q-E space. Instrument settings were different by incident neutron energies, chopper speeds and the resulting choice of energy windows. The energy windows with maximum energy transfer of E = 2.01 meV, 11.7 meV, 12.5 meV, 17.4 meV and 22.1 meV were used. The most relevant data were obtained with the E = 2.01 meV (resolution at the elastic line of 160 μeV) and 11.7 meV (resolution at the elastic line of 500 μeV) windows, which captured the low and intermediate energy excitations in the system. All data were corrected for empty can and vanadium measurements. The data were also scaled by the measured sample weights. The 2.01 meV and 11.7 meV energy scans shown here were obtained by summing up to Q = 0.7 Å^{-1} and Q = 1.8 Å^{-1}, respectively.

Magnetic Measurements: All handling of sample **1** in preparation of magnetic measurements was executed with a Teflon-coated spatula. A crushed crystalline sample of **1** was loaded into a 7 mm diameter quartz tube and was coated with sufficient eicosane to restrain the sample. The quartz tube was fitted with a sealable hose-adapter, evacuated on a Schlenk line, and then flame-sealed under vacuum. Magnetic susceptibility measurements were performed using a MPMSXL SQUID magnetometer (Quantum Design, Inc., San Diego, CA, USA). Dc magnetic susceptibility measurements were performed at temperatures ranging from 2 to 300 K (variable temperature) at 1 T and the magnetization was measured in fields ranging from 0 to 7 T at fixed temperatures. All data were corrected for diamagnetic contributions from the eicosane and for diamagnetism estimated using Pascal's constants [65].

6. Conclusions

In conclusion, we have discussed the challenges and perspectives of neutron scattering in lanthanide-based molecular magnets. The focus of the discussion was on the poly-nuclear clusters with low local symmetry, which present inherent challenges for an experimentalist: a situation of having little data, but many parameters in the effective Hamiltonian, and stiff, parameter-free ab initio calculations.

In the second part of the paper, we presented original results of an inelastic neutron scattering (INS) study on a high blocking temperature single molecule magnet (SMM), its Y^{III} analogue and a non-SMM parent compound. In the parent compound, we observed two peaks, I at 0.75(2) meV and II at 5.2(2) meV. Together with a simple, but plausible Ising spin model suggested by point-charge calculations, peak I allowed us to clarify the low-energy behavior of the material, notably the single-ion ground states, an approximate $M_J \approx \pm 6$ pseudo doublet, and the exchange interaction $\mathcal{J} = -0.12$ K. The physical picture thus obtained, fits well to the low temperature magnetization data without the need for introducing any further parameters. However, additional intermediate- and higher-energy data are needed to fully describe the system. To the best of our knowledge, this is the first time the exchange interaction between lanthanide ions was *directly* determined based upon INS.

In the SMM compound, we observed, among several phonon peaks, a very weak magnetic excitation at 9.2(2) meV. The assignment of the peak to the exchange-split level within the Ising model results in the exchange interaction value of $\mathcal{J} = -17$ K, which does not reproduce the susceptibility curve. We showed that within the Ising model a larger interaction of $\mathcal{J} = -48$ K is required for this, together with an intermolecular exchange of $\mathcal{J}' = -0.02$ K. The reason for the discrepancy between the INS and susceptibility data is at present not clear, but it points to the necessity for a more complex model and additional data points required for its validation.

Supplementary Materials: The following are available online at www.mdpi.com/2312-7481/2/4/45/s1, Figure S1: Low-energy $S(Q,\omega)$ spectrum of the parent compound **1**; Figure S2: Intermediate-energy $S(Q,\omega)$ spectrum of the parent compound **1**; Figure S3: INS spectra of compounds **1**, **2** and **3** with the lattice contributions estimated by the Bose correction procedure.

Acknowledgments: K.P. and O.W. thank J. Mutschler for help with point-charge model calculations. W.J.E. thanks the U.S. National Science Foundation for support (CHE-1565776). The work performed at University of California, Berkeley was supported by the National Science Foundation (NSF) under Grant CHE-1464841.

Author Contributions: O.W. and J.N. conceived and designed the INS experiments; S.D. and J.R.L. conceived and designed the magnetic susceptibility measurements; J.F.C. and W.J.E. contributed samples; O.W., J.N., T.G. and S.D. performed the experiments; K.P., J.N. and O.W. analyzed the data; K.P. and O.W. wrote the core of the paper and all authors contributed to revising it.

Conflicts of Interest: The authors declare no conflict of interest.

References and Notes

1. Rinehart, J.D.; Fang, M.; Evans, W.J.; Long, J.R. A N_2^{3-} Radical-Bridged Terbium Complex Exhibiting Magnetic Hysteresis at 14 K. *J. Am. Chem. Soc.* **2011**, *133*, 14236–14239. [CrossRef] [PubMed]
2. Rinehart, J.D.; Fang, M.; Evans, W.J.; Long, J.R. Strong exchange and magnetic blocking in N_2^{3-}-radical-bridged lanthanide complexes. *Nat. Chem.* **2011**, *3*, 538–542. [CrossRef] [PubMed]
3. Chen, Y.-C.; Liu, J.-L.; Ungur, L.; Liu, J.; Li, Q.-W.; Wang, L.-F.; Ni, Z.-P.; Chibotaru, L.F.; Chen, X.-M.; Tong, M.-L. Symmetry-Supported Magnetic Blocking at 20 K in Pentagonal Bipyramidal Dy(III) Single-Ion Magnets. *J. Am. Chem. Soc.* **2016**, *138*, 2829–2837. [CrossRef] [PubMed]
4. Ungur, L.; Lin, S.-Y.; Tang, J.; Chibotaru, L.F. Single-molecule toroics in Ising-type lanthanide molecular clusters. *Chem. Soc. Rev.* **2014**, *43*, 6894–6905. [CrossRef] [PubMed]
5. Sharples, J.W.; Collison, D.; McInnes, E.J.L.; Schnack, J.; Palacios, E.; Evangelisti, M. Quantum signatures of a molecular nanomagnet in direct magnetocaloric measurements. *Nat. Commun.* **2014**, *5*, 5321. [CrossRef] [PubMed]
6. Shiddiq, M.; Komijani, D.; Duan, Y.; Gaita-Ariño, A.; Coronado, E.; Hill, S. Enhancing coherence in molecular spin qubits via atomic clock transitions. *Nature* **2016**, *531*, 348–351. [CrossRef] [PubMed]
7. Tang, J.; Hewitt, I.; Madhu, N.T.; Chastanet, G.; Wernsdorfer, W.; Anson, C.E.; Benelli, C.; Sessoli, R.; Powell, A.K. Dysprosium Triangles Showing Single-Molecule Magnet Behavior of Thermally Excited Spin States. *Angew. Chem. Int. Ed.* **2006**, *45*, 1729–1733. [CrossRef] [PubMed]
8. Chibotaru, L.F.; Ungur, L.; Soncini, A. The Origin of Nonmagnetic Kramers Doublets in the Ground State of Dysprosium Triangles: Evidence for a Toroidal Magnetic Moment. *Angew. Chem. Int. Ed.* **2008**, *47*, 4126–4129. [CrossRef] [PubMed]
9. Luis, F.; Repollés, A.; Martínez-Pérez, M.J.; Aguilà, D.; Roubeau, O.; Zueco, D.; Alonso, P.J.; Evangelisti, M.; Camón, A.; Sesé, J.; et al. Molecular Prototypes for Spin-Based CNOT and SWAP Quantum Gates. *Phys. Rev. Lett.* **2011**, *107*, 117203. [CrossRef] [PubMed]
10. Rinehart, J.D.; Long, J.R. Exploiting single-ion anisotropy in the design of f-element single-molecule magnets. *Chem. Sci.* **2011**, *2*, 2078–2085. [CrossRef]
11. Ungur, L.; Chibotaru, L.F. Strategies toward High-Temperature Lanthanide-Based Single-Molecule Magnets. *Inorg. Chem.* **2016**, *55*, 10043–10056. [CrossRef] [PubMed]
12. Woodruff, D.N.; Winpenny, R.E.P.; Layfield, R.A. Lanthanide Single-Molecule Magnets. *Chem. Rev.* **2013**, *113*, 5110–5148. [CrossRef] [PubMed]
13. Tang, J.; Zhang, P. *Lanthanide Single Molecule Magnets*, 1st ed.; Springer: Berlin/Heidelberg, Germany, 2015.

14. Liddle, S.T.; van Slageren, J. Improving *f*-element single molecule magnets. *Chem. Soc. Rev.* **2015**, *44*, 6655–6669. [CrossRef] [PubMed]
15. Sessoli, R.; Powell, A.K. Strategies towards single molecule magnets based on lanthanide ions. *Coord. Chem. Rev.* **2009**, *253*, 2328–2341. [CrossRef]
16. Jensen, J.; Mackintosh, A.R. *Rare Earth Magnetism*; Clarendon Press: Oxford, UK, 1991.
17. Newman, D.J. Theory of lanthanide crystal fields. *Adv. Phys.* **1971**, *20*, 197–256. [CrossRef]
18. Christou, G.; Gatteschi, D.; Hendrickson, D.N.; Sessoli, R. Single-Molecule Magnets. *MRS Bull.* **2000**, *25*, 66–71. [CrossRef]
19. Gatteschi, D.; Sessoli, R. Quantum Tunneling of Magnetization and Related Phenomena in Molecular Materials. *Angew. Chem. Int. Ed.* **2003**, *42*, 268–297. [CrossRef] [PubMed]
20. Ishikawa, N.; Sugita, M.; Ishikawa, T.; Koshihara, S.; Kaizu, Y. Lanthanide Double-Decker Complexes Functioning as Magnets at the Single-Molecular Level. *J. Am. Chem. Soc.* **2003**, *125*, 8694–8695. [CrossRef] [PubMed]
21. Waldmann, O. A Criterion for the Anisotropy Barrier in Single-Molecule Magnets. *Inorg. Chem.* **2007**, *46*, 10035–10037. [CrossRef] [PubMed]
22. Pedersen, K.S.; Woodruff, D.N.; Bendix, J.; Clérac, R. Experimental Aspects of Lanthanide Single-Molecule Magnet Physics. In *Lanthanides and Actinides in Molecular Magnetism*; Wiley-VCH Verlag GmbH & Co. KGaA: Weinheim, Germany, 2015; pp. 125–152.
23. Furrer, A.; Waldmann, O. Magnetic cluster excitations. *Rev. Mod. Phys.* **2013**, *85*, 367–420. [CrossRef]
24. Clemente-Juan, J.M.; Coronado, E.; Gaita-Ariño, A. Mononuclear Lanthanide Complexes: Use of the Crystal Field Theory to Design Single-Ion Magnets and Spin Qubits. In *Lanthanides and Actinides in Molecular Magnetism*; Wiley-VCH Verlag GmbH & Co. KGaA: Weinheim, Germany, 2015; pp. 27–60.
25. Sorace, L.; Gatteschi, D. Electronic Structure and Magnetic Properties of Lanthanide Molecular Complexes. In *Lanthanides and Actinides in Molecular Magnetism*; Wiley-VCH Verlag GmbH & Co. KGaA: Weinheim, Germany, 2015; pp. 1–26.
26. Klokishner, S.I.; Ostrovsky, S.M.; Reu, O.S.; Palii, A.V.; Tregenna-Piggott, P.L.W.; Brock-Nannestad, T.; Bendix, J.; Mutka, H. Magnetic Anisotropy in the $[Cu^{II}LTb^{III}(hfac)_2]_2$ Single Molecule Magnet: Experimental Study and Theoretical Modeling. *J. Phys. Chem. C* **2009**, *113*, 8573–8582. [CrossRef]
27. Magnani, N.; Caciuffo, R.; Colineau, E.; Wastin, F.; Baraldi, A.; Buffagni, E.; Capelletti, R.; Carretta, S.; Mazzera, M.; Adroja, D.T.; et al. Low-energy spectrum of a Tm-based double-decker complex. *Phys. Rev. B* **2009**, *79*, 104407. [CrossRef]
28. Dreiser, J.; Pedersen, K.S.; Piamonteze, C.; Rusponi, S.; Salman, Z.; Ali, M.E.; Schau-Magnussen, M.; Thuesen, C.A.; Piligkos, S.; Weihe, H.; et al. Direct observation of a ferri-to-ferromagnetic transition in a fluoride-bridged 3d-4f molecular cluster. *Chem. Sci.* **2012**, *3*, 1024–1032. [CrossRef]
29. Kofu, M.; Yamamuro, O.; Kajiwara, T.; Yoshimura, Y.; Nakano, M.; Nakajima, K.; Ohira-Kawamura, S.; Kikuchi, T.; Inamura, Y. Hyperfine structure of magnetic excitations in a Tb-based single-molecule magnet studied by high-resolution neutron spectroscopy. *Phys. Rev. B* **2013**, *88*, 64405. [CrossRef]
30. Marx, R.; Moro, F.; Dorfel, M.; Ungur, L.; Waters, M.; Jiang, S.D.; Orlita, M.; Taylor, J.; Frey, W.; Chibotaru, L.F.; et al. Spectroscopic determination of crystal field splittings in lanthanide double deckers. *Chem. Sci.* **2014**, *5*, 3287–3293. [CrossRef]
31. Baker, M.L.; Tanaka, T.; Murakami, R.; Ohira-Kawamura, S.; Nakajima, K.; Ishida, T.; Nojiri, H. Relationship between Torsion and Anisotropic Exchange Coupling in a Tb^{III}-Radical-Based Single-Molecule Magnet. *Inorg. Chem.* **2015**, *54*, 5732–5738. [CrossRef] [PubMed]
32. Pedersen, K.S.; Ungur, L.; Sigrist, M.; Sundt, A.; Schau-Magnussen, M.; Vieru, V.; Mutka, H.; Rols, S.; Weihe, H.; Waldmann, O.; et al. Modifying the properties of 4f single-ion magnets by peripheral ligand functionalisation. *Chem. Sci.* **2014**, *5*, 1650–1660. [CrossRef]
33. Kettles, F.J.; Milway, V.A.; Tuna, F.; Valiente, R.; Thomas, L.H.; Wernsdorfer, W.; Ochsenbein, S.T.; Murrie, M. Exchange Interactions at the Origin of Slow Relaxation of the Magnetization in $\{TbCu_3\}$ and $\{DyCu_3\}$ Single-Molecule Magnets. *Inorg. Chem.* **2014**, *53*, 8970–8978. [CrossRef] [PubMed]
34. Giansiracusa, M.J.; Vonci, M.; Van den Heuvel, W.; Gable, R.W.; Moubaraki, B.; Murray, K.S.; Yu, D.; Mole, R.A.; Soncini, A.; Boskovic, C. Carbonate-Bridged Lanthanoid Triangles: Single-Molecule Magnet Behavior, Inelastic Neutron Scattering, and Ab Initio Studies. *Inorg. Chem.* **2016**, *55*, 5201–5214. [CrossRef] [PubMed]

35. Vonci, M.; Giansiracusa, M.J.; Gable, R.W.; Van den Heuvel, W.; Latham, K.; Moubaraki, B.; Murray, K.S.; Yu, D.; Mole, R.A.; Soncini, A.; et al. Ab initio calculations as a quantitative tool in the inelastic neutron scattering study of a single-molecule magnet analogue. *Chem. Commun.* **2016**, *52*, 2091–2094. [CrossRef] [PubMed]
36. Buschow, K.H.J.; de Boer, F.R. *Physics of Magnetism and Magnetic Materials*, 1st ed.; Kluver Academic/Plenum Publishers: New York, NY, USA, 2003.
37. Blagg, R.J.; Ungur, L.; Tuna, F.; Speak, J.; Comar, P.; Collison, D.; Wernsdorfer, W.; McInnes, E.J.L.; Chibotaru, L.F.; Winpenny, R.E.P. Magnetic relaxation pathways in lanthanide single-molecule magnets. *Nat. Chem* **2013**, *5*, 673–678. [CrossRef] [PubMed]
38. Demir, S.; Jeon, I.-R.; Long, J.R.; Harris, T.D. Radical ligand-containing single-molecule magnets. *Coord. Chem. Rev.* **2015**, *289–290*, 149–176. [CrossRef]
39. Bewley, R.I.; Taylor, J.W.; Bennington, S.M. LET, a cold neutron multi-disk chopper spectrometer at ISIS. *Nucl. Instrum. Methods Phys. Res. Sect. A Accel. Spectrom. Detect. Assoc. Equip.* **2011**, *637*, 128–134. [CrossRef]
40. Konstantatos, A.; Bewley, R.; Barra, A.-L.; Bendix, J.; Piligkos, S.; Weihe, H. In-Depth Magnetic Characterization of a [2 × 2] Mn(III) Square Grid Using SQUID Magnetometry, Inelastic Neutron Scattering, and High-Field Electron Paramagnetic Resonance Spectroscopy. *Inorg. Chem.* **2016**, *55*, 10377–10382. [CrossRef] [PubMed]
41. Woolfson, R.J.; Timco, G.A.; Chiesa, A.; Vitorica-Yrezabal, I.J.; Tuna, F.; Guidi, T.; Pavarini, E.; Santini, P.; Carretta, S.; Winpenny, R.E.P. $[CrF(O_2C^tBu)_2]_9$: Synthesis and Characterization of a Regular Homometallic Ring with an Odd Number of Metal Centers and Electrons. *Angew. Chem. Int. Ed.* **2016**, *55*, 8856–8859. [CrossRef] [PubMed]
42. EPR (and photon-based spectroscopy in general) is subject to the selection rules $\Delta M = \pm 1$ and $\Delta S = 0$, and INS to the rules $\Delta M = 0, \pm 1$ and $\Delta S = 0, \pm 1$. The selection rules of transitions within or between J multiplets are obtained by replacing $M \rightarrow M_J$, $S \rightarrow J$.
43. Moreno Pineda, E.; Chilton, N.F.; Marx, R.; Dörfel, M.; Sells, D.O.; Neugebauer, P.; Jiang, S.-D.; Collison, D.; van Slageren, J.; McInnes, E.J.L.; et al. Direct measurement of dysprosium(III)-dysprosium(III) interactions in a single-molecule magnet. *Nat. Commun.* **2014**, *5*, 5243. [CrossRef] [PubMed]
44. Dreiser, J.; Pedersen, K.S.; Schnegg, A.; Holldack, K.; Nehrkorn, J.; Sigrist, M.; Tregenna-Piggott, P.; Mutka, H.; Weihe, H.; Mironov, V.S.; et al. Three-Axis Anisotropic Exchange Coupling in the Single-Molecule Magnets $NEt_4[Mn^{III}{}_2(5\text{-Brsalen})_2(MeOH)_2M^{III}(CN)_6]$ (M = Ru, Os). *Chem. Eur. J.* **2013**, *19*, 3693–3701. [CrossRef] [PubMed]
45. Koehler, W.C.; Moon, R.M.; Cable, J.W.; Child, H.R. Neutron scattering experiments on gadolinium. *J. Phys. Colloq.* **1971**, *32*, C1-296–C1-298. [CrossRef]
46. Yu, J.; LeClair, P.R.; Mankey, G.J.; Robertson, J.L.; Crow, M.L.; Tian, W. Exploring the magnetic phase diagram of dysprosium with neutron diffraction. *Phys. Rev. B* **2015**, *91*, 14404. [CrossRef]
47. Sears, V.F. Neutron scattering lengths and cross sections. *Neutron News* **1992**, *3*, 26–37. [CrossRef]
48. Dreiser, J.; Waldmann, O.; Dobe, C.; Carver, G.; Ochsenbein, S.T.; Sieber, A.; Güdel, H.U.; van Duijn, J.; Taylor, J.; Podlesnyak, A. Quantized antiferromagnetic spin waves in the molecular Heisenberg ring $CsFe_8$. *Phys. Rev. B* **2010**, *81*, 24408. [CrossRef]
49. Ungur, L.; Chibotaru, L.F. Computational Modelling of the Magnetic Properties of Lanthanide Compounds. In *Lanthanides and Actinides in Molecular Magnetism*; Wiley-VCH Verlag GmbH & Co. KGaA: Weinheim, Germany, 2015; pp. 153–184.
50. Furrer, A.; Güdel, H.U.; Blank, H.; Heidemann, A. Direct Observation of Exchange Splittings in $Cs_3Tb_2Br_9$ by Neutron Spectroscopy. *Phys. Rev. Lett.* **1989**, *62*, 210–213. [CrossRef] [PubMed]
51. Furrer, A.; Güdel, H.U.; Krausz, E.R.; Blank, H. Neutron spectroscopic study of anisotropic exchange in the dimer compound $Cs_3Ho_2Br_9$. *Phys. Rev. Lett.* **1990**, *64*, 68–71. [CrossRef] [PubMed]
52. Guo, Y.-N.; Ungur, L.; Granroth, G.E.; Powell, A.K.; Wu, C.; Nagler, S.E.; Tang, J.; Chibotaru, L.F.; Cui, D. An NCN-pincer ligand dysprosium single-ion magnet showing magnetic relaxation via the second excited state. *Sci. Rep.* **2014**, *4*, 5471. [CrossRef] [PubMed]
53. Hutchings, M.T. Point-Charge Calculations of Energy Levels of Magnetic Ions in Crystalline Electric Fields. In *Solid State Physics*; Seitz, F., Turnbull, D., Eds.; Elsevier B.V.: Amsterdam, The Netherlands, 1964; Volume 16, pp. 227–273.

54. Baker, M.L.; Guidi, T.; Carretta, S.; Ollivier, J.; Mutka, H.; Gudel, H.U.; Timco, G.A.; McInnes, E.J.L.; Amoretti, G.; Winpenny, R.E.P.; et al. Spin dynamics of molecular nanomagnets unravelled at atomic scale by four-dimensional inelastic neutron scattering. *Nat. Phys.* **2012**, *8*, 906–911. [CrossRef]
55. Guidi, T.; Gillon, B.; Mason, S.A.; Garlatti, E.; Carretta, S.; Santini, P.; Stunault, A.; Caciuffo, R.; van Slageren, J.; Klemke, B.; et al. Direct observation of finite size effects in chains of antiferromagnetically coupled spins. *Nat. Commun.* **2015**, *6*, 7061. [CrossRef] [PubMed]
56. Waldmann, O.; Bircher, R.; Carver, G.; Sieber, A.; Güdel, H.U.; Mutka, H. Exchange-coupling constants, spin density map, and Q dependence of the inelastic neutron scattering intensity in single-molecule magnets. *Phys. Rev. B* **2007**, *75*, 174438. [CrossRef]
57. Borta, A.; Gillon, B.; Gukasov, A.; Cousson, A.; Luneau, D.; Jeanneau, E.; Ciumacov, I.; Sakiyama, H.; Tone, K.; Mikuriya, M. Local magnetic moments in a dinuclear Co^{2+} complex as seen by polarized neutron diffraction: Beyond the effective spin-1/2 model. *Phys. Rev. B* **2011**, *83*, 184429. [CrossRef]
58. Zaharko, O.; Pregelj, M.; Zorko, A.; Podgajny, R.; Gukasov, A.; van Tol, J.; Klokishner, S.I.; Ostrovsky, S.; Delley, B. Source of magnetic anisotropy in quasi-two-dimensional XY $\{Cu_4(tetrenH_5)W(CN)_8]_4 \cdot 7.2\ H_2O\}_n$ bilayer molecular magnet. *Phys. Rev. B* **2013**, *87*, 24406. [CrossRef]
59. Ridier, K.; Gillon, B.; Gukasov, A.; Chaboussant, G.; Cousson, A.; Luneau, D.; Borta, A.; Jacquot, J.-F.; Checa, R.; Chiba, Y.; et al. Polarized Neutron Diffraction as a Tool for Mapping Molecular Magnetic Anisotropy: Local Susceptibility Tensors in CoII Complexes. *Chem. Eur. J.* **2016**, *22*, 724–735. [CrossRef] [PubMed]
60. Ridier, K.; Mondal, A.; Boilleau, C.; Cador, O.; Gillon, B.; Chaboussant, G.; Le Guennic, B.; Costuas, K.; Lescouëzec, R. Polarized Neutron Diffraction to Probe Local Magnetic Anisotropy of a Low-Spin Fe(III) Complex. *Angew. Chem. Int. Ed.* **2016**, *55*, 3963–3967. [CrossRef] [PubMed]
61. Evans, W.J.; Lee, D.S.; Rego, D.B.; Perotti, J.M.; Kozimor, S.A.; Moore, E.K.; Ziller, J.W. Expanding Dinitrogen Reduction Chemistry to Trivalent Lanthanides via the LnZ_3/Alkali Metal Reduction System: Evaluation of the Generality of Forming $Ln_2(\mu\text{-}\eta^2\text{:}\eta^2\text{-}N_2)$ Complexes via LnZ_3/K. *J. Am. Chem. Soc.* **2004**, *126*, 14574–14582. [CrossRef] [PubMed]
62. Schnack, J. Influence of intermolecular interactions on magnetic observables. *Phys. Rev. B* **2016**, *93*, 54421. [CrossRef]
63. Albuquerque, A.F.; Alet, F.; Corboz, P.; Dayal, P.; Feiguin, A.; Fuchs, S.; Gamper, L.; Gull, E.; Gürtler, S.; Honecker, A.; et al. The ALPS project release 1.3: Open-source software for strongly correlated systems. *J. Magn. Magn. Mater.* **2007**, *310*, 1187–1193. [CrossRef]
64. Bauer, B.; Carr, L.D.; Evertz, L.D.; Feiguin, A.; Freire, J.; Fuchs, S.; Gamper, L.; Gukelberger, J.; Gull, E.; Guertler, S.; et al. The ALPS project release 2.0: Open source software for strongly correlated systems. *J. Stat. Mech. Theory Exp.* **2011**, *2011*, P05001. [CrossRef]
65. Bain, G.A.; Berry, J.F. Diamagnetic Corrections and Pascal's Constants. *J. Chem. Educ.* **2008**, *85*, 532. [CrossRef]

© 2016 by the authors; licensee MDPI, Basel, Switzerland. This article is an open access article distributed under the terms and conditions of the Creative Commons Attribution (CC-BY) license (http://creativecommons.org/licenses/by/4.0/).